



Supplement of

Iron from coal combustion particles dissolves much faster than mineral dust under simulated atmospheric acidic conditions

Clarissa Baldo et al.

Correspondence to: Zongbo Shi (z.shi@bham.ac.uk) and Akinori Ito (akinorii@jamstec.go.jp)

The copyright of individual parts of the supplement might differ from the article licence.

Text S1: Description of the microwave digestion method

“1-3 mg of dust/ash were weighed on quartz filters (1.5 cm² punch). The filters were placed into vessels with 10 ml of 68% ultrapure nitric acid (HNO₃, Romil). The vessels were loaded into a MARS 6 Microwave Digestion System (CEM Technology). The filter-membrane programme was used to digest the samples. This consists of an increase in temperature to 200°C (15-min ramp time) followed by 15 min at 200°C and pressure 800 psi. The sample solutions were then diluted to 2% HNO₃ and filtered through 0.45 µm membrane filters. The samples were stored in the fridge at 4°C prior the analysis. The Fe concentration in the filtrates was measured by inductively coupled plasma mass spectrometry (ICP-MS) analysis.

After each digestion, the vessels were cleaned to prevent contamination. These were first washed with DI water and dried in the oven at 70°C. Subsequently, 10 ml of concentrated HNO₃ was added to each vessel which were placed into the microwave to undergo the cleaning programme (ramp time of 15 min to 190°C, followed by 10 min at 190°C and pressure 800 psi). Finally, the vessels were rinsed with DI water and air-dried in a fume hood. All glassware was acid washed in 10% HNO₃.

To assess the recovery of Fe, we used a standard reference material for urban particulate matter (1 mg of NIST SRM 1648A on quartz filter). The recovery of Fe from NIST was 89.0% ± 0.4%. We used the Arizona Test Dust (ATD, Iso 12103-1, Power Technology, Inc.) to test the method. The estimated total Fe content in the ATD was 3.501% ± 0.056% which is comparable with the latest consensus value for the total Fe in ATD. Here, the estimated recovery of Fe from the ATD samples calculated using the reference total Fe in ATD and the total Fe in the ATD samples obtained in this study (prior the correction for the Fe recovery based on the NIST results) is 94.0% ± 1.5%”.

25 Table S1: Summary of the Fe dissolution experiments conducted in this study. A particles/liquid ratio of 1 g L⁻¹ was used at different experimental conditions. The molar concentrations of H₂SO₄, H₂C₂O₄ and (NH₄)₂SO₄ in the experiment solutions are reported (mol L⁻¹). The molar concentration and activity (a) of H⁺ and the solution pH before adding the samples (i) and at the end of the experiments (f) were calculated using the E-AIM model III for aqueous solution (Wexler and Clegg, 2002). The estimated buffered H⁺ is ~0.008 M for Krakow ash, ~0.0007 M for Aberthaw/Shandong ash, ~0.004 M for Libyan dust end member (the procedure used to calculate the sample buffer capacity is reported in section 2.2). The final pH (pH_f) accounts for the buffer capacity of the CFA samples. For the experiment solutions with no (NH₄)₂SO₄, the initial pH (pH_i) and pH_f were also measured

30

	Exp.	[H ₂ SO ₄]	[(NH ₄) ₂ SO ₄]	[H ₂ C ₂ O ₄]	Model estimates						Measured pH	
					[H ⁺] _i	[H ⁺] _f	a(H ⁺) _i	a(H ⁺) _f	pH _i	pH _f	pH _i	pH _f
Krakow ash	Exp 1	0.01	-	-	0.016	0.009	0.86	0.86	1.9	2.1	1.9	2.1
	Exp 2	0.05	1	-	0.031	0.029	0.29	0.29	2.0	2.1	0.0	-
	Exp 3	0.05	1	0.01	0.035	0.032	0.29	0.29	2.0	2.0	0.0	-
	Exp 4	0.01	-	0.01	0.023	0.016	0.86	0.85	1.7	1.9	1.7	1.9
	Exp 1	0.005	-	-	0.008	0.002	0.89	0.88	2.1	2.7	2.2	2.6
	Exp 2	0.01	1	-	0.006	0.004	0.28	0.28	2.8	3.0	0.0	-
	Exp 3	0.005	1	0.01	0.007	0.005	0.28	0.28	2.7	2.9	0.0	-
	Exp 5	0.1	-	0.03	0.138	0.131	0.76	0.76	1.0	1.0	1.1	1.1
	Exp 6	0.25	0.5	0.03	0.189	0.186	0.49	0.49	1.0	1.0	0.0	-
	Exp 7	0.35	1	0.03	0.252	0.249	0.39	0.39	1.0	1.0	0.0	-
Exp 8	0.4	1.5	0.03	0.285	0.282	0.33	0.33	1.0	1.0	0.0	-	
Aberthaw ash	Exp 1	0.005	-	-	0.008	0.008	0.89	0.89	2.1	2.2	2.1	2.3
	Exp 2	0.05	1	-	0.031	0.031	0.29	0.29	2.0	2.0	0.0	-
	Exp 3	0.05	1	0.01	0.035	0.034	0.29	0.29	2.0	2.0	0.0	-
	Exp 4	0.002	-	0.01	0.012	0.011	0.90	0.90	2.0	2.0	2.0	2.1
	Exp 1	0.001	-	-	0.002	0.001	0.94	0.94	2.8	2.9	2.8	3.1
	Exp 2	0.005	1	-	0.003	0.003	0.28	0.28	3.1	3.1	0.0	-
Shandong ash	Exp 1	0.005	-	-	0.008	0.008	0.89	0.89	2.1	2.2	2.1	2.2
	Exp 2	0.05	1	-	0.031	0.031	0.29	0.29	2.0	2.0	0.0	-
	Exp 3	0.05	1	0.01	0.035	0.034	0.29	0.29	2.0	2.0	0.0	-
	Exp 4	0.002	-	0.01	0.012	0.011	0.90	0.90	2.0	2.0	2.0	2.0
	Exp 1	0.001	-	-	0.002	0.001	0.94	0.94	2.8	2.9	2.8	3.1
	Exp 2	0.005	1	-	0.003	0.003	0.28	0.28	3.1	3.1	0.0	-
Libyan dust	Exp 1	0.01	-	-	0.016	0.012	0.86	0.86	1.9	2.0	1.9	2.0
	Exp 2	0.05	1	-	0.031	0.030	0.29	0.29	2.0	2.1	0.0	-
	Exp 3	0.05	1	0.01	0.035	0.033	0.29	0.29	2.0	2.0	0.0	-
	Exp 4	0.005	-	0.01	0.016	0.012	0.88	0.87	1.9	2.0	1.9	2.0

35 **Table S2: Percentages of ascorbate Fe (FeA), dithionite Fe (FeD), magnetite Fe (FeM), and total Fe (FeT) in the Arizona Test Dust (ATD, Iso 12103-1, Power Technology, Inc.) to the total dust mass (wt%). For each type of extracted Fe, the standard deviation (SD), relative standard deviations (RSD), and number of replicates (n) is reported.**

Fe species	wt%	SD	RSD (%)	n
FeA	0.057	0.002	3	7
FeD	0.394	0.045	11	7
FeM	0.047	0.006	12	7
FeT	3.501	0.056	2	3

Table S3: Summary of the molar concentration in mol L⁻¹ and activity (a) of total oxalate ions, C₂O₄²⁻, and HC₂O₄⁻ in the experiment solutions calculated using the E-AIM model III for aqueous solution (Wexler and Clegg, 2002). A comprehensive description of the experimental conditions is provided in Table S1. pH_f is the calculated final pH in the experiment solutions.

Sample	Exp.	pH _f	[oxalate] _{total}	[C ₂ O ₄ ²⁻]	a(C ₂ O ₄ ²⁻)	[HC ₂ O ₄ ⁻]	a(HC ₂ O ₄ ⁻)
Krakow ash	Exp 3	2.0	0.009	0.00071	0.04	0.009	0.55
Krakow ash	Exp 4	1.9	0.008	0.00006	0.49	0.008	0.86
Krakow ash	Exp 3	2.9	0.010	0.00343	0.04	0.006	0.54
Krakow ash	Exp 5	1.0	0.012	0.00002	0.22	0.012	0.79
Krakow ash	Exp 6	1.0	0.015	0.00010	0.06	0.015	0.64
Krakow ash	Exp 7	1.0	0.015	0.00015	0.04	0.015	0.65
Krakow ash	Exp 8	1.0	0.015	0.00022	0.03	0.015	0.68
Aberthaw ash	Exp 3	2.0	0.009	0.00066	0.04	0.009	0.56
Aberthaw ash	Exp 4	2.0	0.009	0.00007	0.60	0.009	0.90
Shandong ash	Exp 3	2.0	0.009	0.00066	0.04	0.009	0.56
Shandong ash	Exp 4	2.0	0.009	0.00007	0.60	0.009	0.90
Libyan dust	Exp 3	2.0	0.009	0.00068	0.04	0.009	0.56
Libyan dust	Exp 4	2.0	0.008	0.00006	0.55	0.008	0.88

Table S4: Modelled mass concentration of total Fe in PM_{2.5} aerosol particles (ng m⁻³) over the Bay of Bengal from 27 December 2008 to 26 January 2009. Observations are reported in Bikkina et al. (2020). The concentrations of total Fe were calculated along the cruise tracks in the North Bay of Bengal (27 December 2008 - 10 January 2009) and the South Bay of Bengal (11-26 January 2009) using the IMPACT model. The total Fe emissions from anthropogenic combustion sources (ANTHRO) and biomass burning (BB) were estimated using the emission inventory of (Ito et al., 2018), whereas Fe emissions from mineral dust sources (DUST) were dynamically simulated (Ito et al., 2021).

Date	DUST	ANTHRO	BB	Total Fe
27/12/2008	20.7	11.1	0.2	31.9
28/12/2008	56.8	12.8	0.4	70.0
29/12/2008	71.2	10.7	0.4	82.4
30/12/2008	48.5	11.7	0.5	60.7
31/12/2008	55.3	17.1	0.6	73.0
01/01/2009	65.4	25.2	0.7	91.3
02/01/2009	69.2	33.5	0.7	103.4
03/01/2009	66.8	33.4	0.6	100.8
04/01/2009	48.0	19.1	0.5	67.7
05/01/2009	18.1	9.2	0.4	27.8
06/01/2009	6.5	7.0	0.3	13.9
07/01/2009	36.3	18.9	0.4	55.6
08/01/2009	31.1	14.9	0.4	46.4
09/01/2009	13.9	6.4	0.5	20.8
10/01/2009	3.4	27.9	1.9	33.2
11/01/2009	7.2	35.2	3.8	46.3
12/01/2009	5.6	21.4	3.5	30.5
13/01/2009	3.3	13.6	5.4	22.3
14/01/2009	3.3	15.0	7.0	25.2
15/01/2009	4.2	25.7	4.9	34.8
16/01/2009	4.6	24.3	6.1	35.0
17/01/2009	2.9	15.5	6.4	24.8
18/01/2009	2.0	9.5	4.7	16.1
19/01/2009	1.1	3.4	2.2	6.7
20/01/2009	1.0	4.3	3.9	9.2
21/01/2009	2.3	9.4	2.7	14.3
22/01/2009	2.5	8.7	2.1	13.2
23/01/2009	1.1	4.2	4.3	9.6
24/01/2009	0.7	2.4	5.0	8.1
25/01/2009	0.6	2.9	9.5	13.1
26/01/2009	0.4	2.5	8.2	11.2

50 **Table S5: Modelled Fe solubility in PM_{2.5} aerosol particles (Fe%) over the Bay of Bengal from 27 December 2008 to 26 January 2009. Observations are reported in Bikkina et al. (2020). The aerosol Fe solubility were calculated along the cruise tracks in the North Bay of Bengal (27 December 2008 - 10 January 2009) and the South Bay of Bengal (11-26 January 2009) using the IMPACT model. In Test 0, we run the model without upgrades (Ito et al., 2021) and applying the proton-promoted, oxalate-promoted, and photoinduced dissolution schemes for combustion aerosols in Table S6 (Ito, 2015). The proton + oxalate dissolution scheme (Table 1) was applied in Test 1 and 3, while proton-promoted dissolution is used for Test 2. We adopted the base mineralogy for anthropogenic Fe emissions (Rathod et al., 2020) in Test 1 and 2. In Test 3, the Fe speciation of Krakow ash was used for all combustion sources.**

55

Date	Test 0	Test 1	Test 2	Test 3
27/12/2008	14.2	17.2	38.0	15.2
28/12/2008	8.8	11.1	21.7	10.6
29/12/2008	6.5	9.3	17.2	9.2
30/12/2008	7.5	12.5	25.1	13.2
31/12/2008	7.5	14.4	29.9	14.6
01/01/2009	8.7	16.2	33.2	16.3
02/01/2009	8.8	15.8	34.1	16.0
03/01/2009	8.8	16.5	37.9	16.0
04/01/2009	8.9	16.1	35.7	16.0
05/01/2009	14.0	18.2	40.4	19.2
06/01/2009	21.6	25.2	58.4	26.6
07/01/2009	12.1	17.7	39.6	17.2
08/01/2009	9.5	16.4	36.0	15.6
09/01/2009	10.5	15.9	33.4	16.3
10/01/2009	19.0	26.7	77.9	31.4
11/01/2009	12.8	24.2	74.2	29.3
12/01/2009	16.3	24.7	81.1	30.0
13/01/2009	25.2	24.0	82.8	30.9
14/01/2009	20.5	23.8	86.8	31.1
15/01/2009	12.8	24.4	89.8	30.0
16/01/2009	15.0	24.4	88.6	30.4
17/01/2009	22.8	26.3	90.7	33.2
18/01/2009	32.0	28.2	91.2	35.3
19/01/2009	47.9	28.8	88.7	35.3
20/01/2009	48.7	30.7	94.5	39.9
21/01/2009	36.5	35.7	88.6	42.0
22/01/2009	37.1	37.8	86.7	41.7
23/01/2009	60.9	37.5	95.3	46.8
24/01/2009	73.0	35.7	97.6	47.3
25/01/2009	66.8	32.7	98.8	46.0
26/01/2009	71.6	34.7	99.2	47.7

Table S6: Constants used to calculate the Fe dissolution rates for fossil fuel combustion aerosols in Ito (2015), and the new dissolution scheme implemented in this study. Note that the dissolution scheme in Ito (2015) was based on laboratory measurements conducted at low ionic strength.

Scheme	Reference	Rate constant - $k(\text{pH}, T)^a$		m^c
Proton	Ito (2015)	$5.24 \times 10^{-8} \exp[E(\text{pH})^b \times (1/298 - 1/T)]$		0.36
Oxalate	Ito (2015)	$3.85 \times 10^{-6} \exp[E(\text{pH})^b \times (1/298 - 1/T)]$		1
Photoinduced	Ito (2015)	$4.10 \times 10^{-6} \exp[E(\text{pH})^b \times (1/298 - 1/T)]$		1
Proton	This study	$7.61 \times 10^{-6} \exp[E(\text{pH})^b \times (1/298 - 1/T)]$	Stage I - Kinetic fast	0.241
		$1.91 \times 10^{-7} \exp[E(\text{pH})^b \times (1/298 - 1/T)]$	Stage II - Kinetic intermediate	0.195
		$2.48 \times 10^{-7} \exp[E(\text{pH})^b \times (1/298 - 1/T)]$	Stage III - Kinetic slow	0.843
Proton + Oxalate	This study	$5.54 \times 10^{-6} \exp[E(\text{pH})^b \times (1/298 - 1/T)]$	Stage I - Kinetic fast	0.209
		$1.50 \times 10^{-7} \exp[E(\text{pH})^b \times (1/298 - 1/T)]$	Stage II - Kinetic intermediate	0.091
		$1.77 \times 10^{-8} \exp[E(\text{pH})^b \times (1/298 - 1/T)]$	Stage III - Kinetic slow	0.204

60 ^a $K(\text{pH}, T)$ is the rate constant ($\text{moles Fe g}^{-1} \text{s}^{-1}$) for each dissolution scheme.

^b $E(\text{pH}) = -1.56 \times 10^3 \times \text{pH} + 1.08 \times 10^4$.

^c m_i is the reaction order with respect to aqueous phase protons.

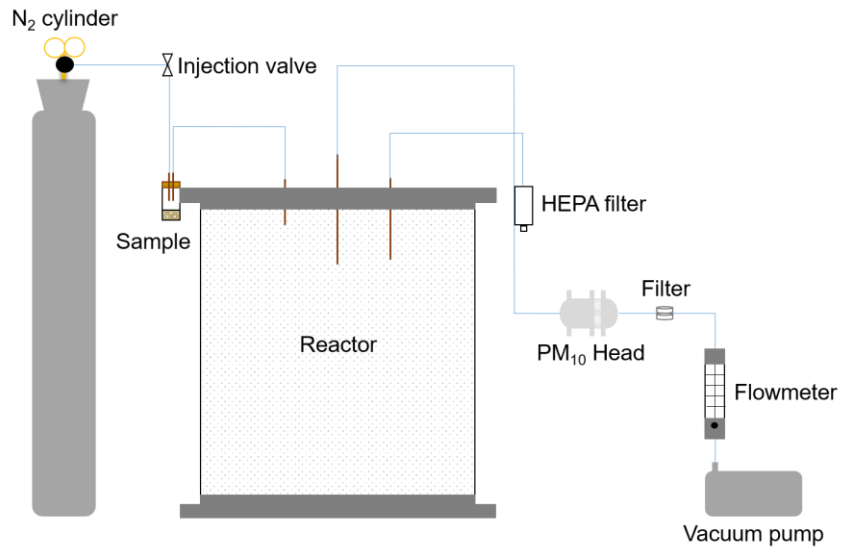


Figure S1: PM₁₀ collection system.

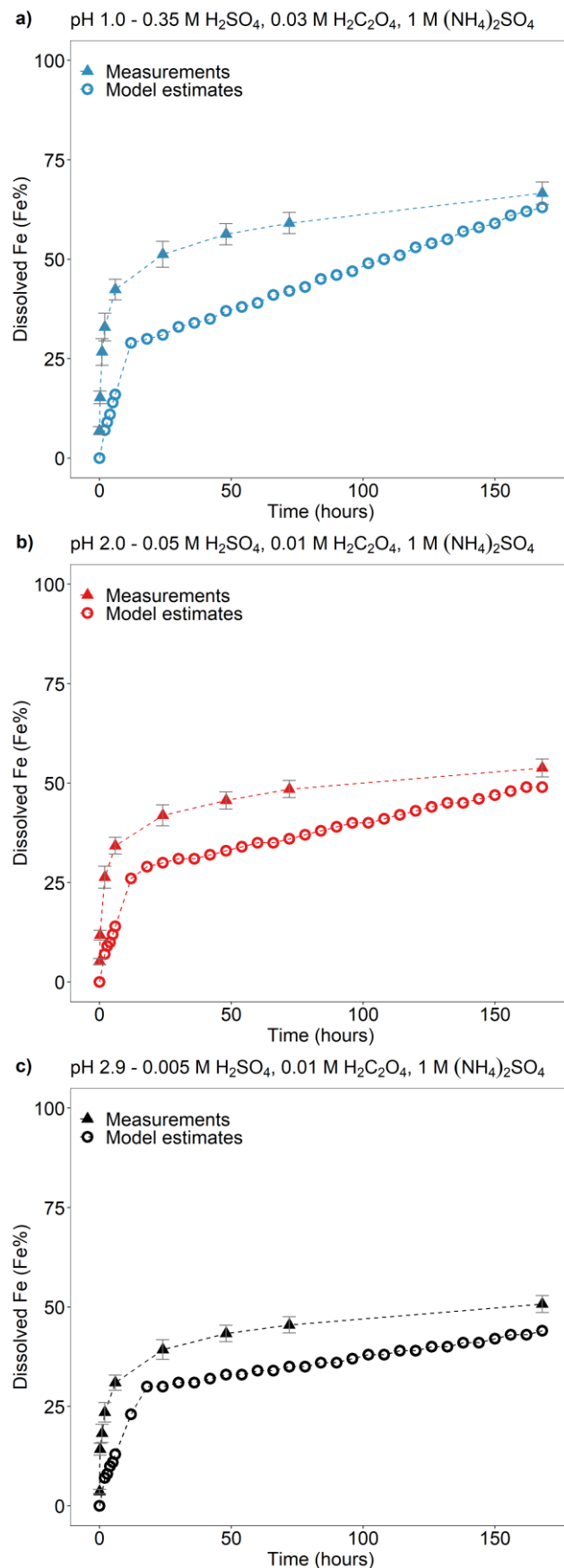
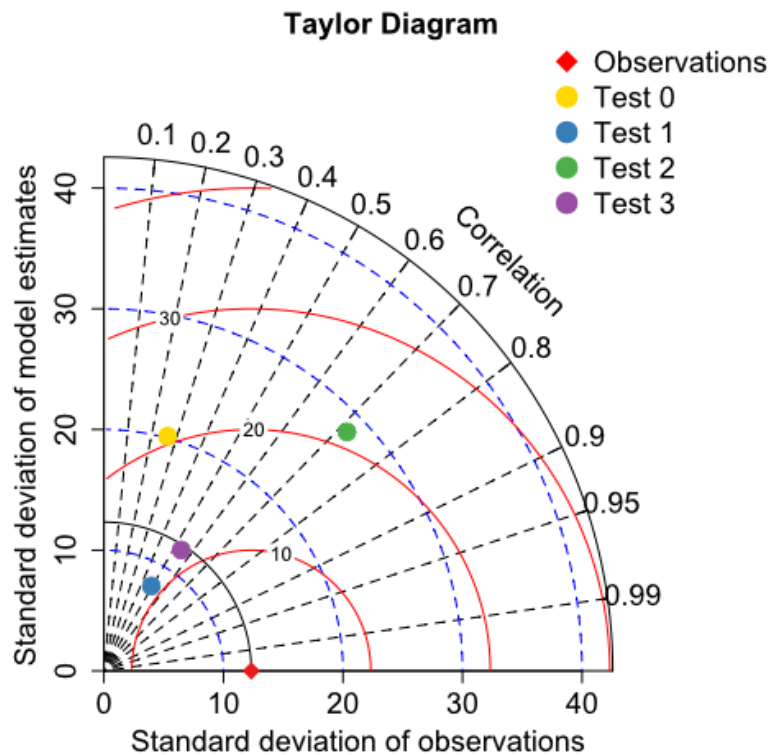
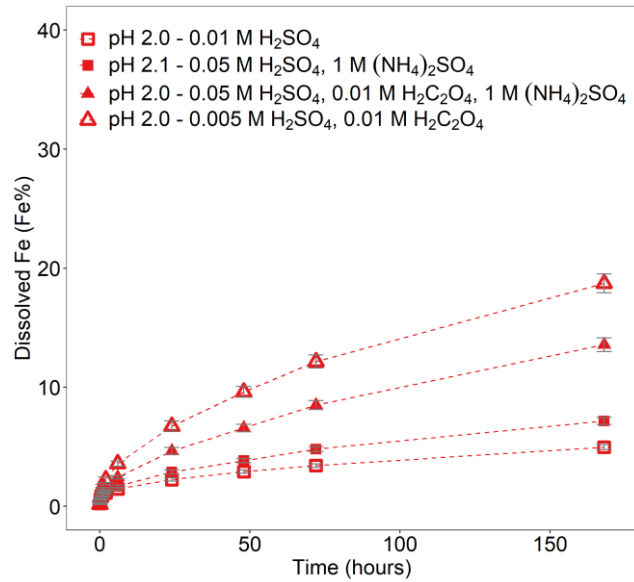


Figure S2: Comparison between the Fe dissolution kinetics of Krakow ash predicted using Eq. (1) and measured in H₂SO₄ solutions a) at pH 1.0 with 0.03 M H₂C₂O₄ and 1 M (NH₄)₂SO₄, b) at pH 2.0 with 0.01 M H₂C₂O₄ and 1 M (NH₄)₂SO₄, c) at pH 2.9 with 0.01 M H₂C₂O₄ and 1 M (NH₄)₂SO₄. The molar concentrations of H₂SO₄, H₂C₂O₄ and (NH₄)₂SO₄ in the experiment solutions are shown. The final pH of the experiment solutions is also reported, which was calculated using the E-AIM model III for aqueous solution (Wexler and Clegg, 2002) accounting for the buffer capacity of the CFA samples (Experiment 7 at pH 1.0, Experiment 3 at pH 2.0, and Experiment 3 at pH 2.9 in Table S1).



80 **Figure S3:** Comparison between observations and model estimates of Fe solubility in $PM_{2.5}$ aerosol particles over the Bay of Bengal from 27 December 2008 to 26 January 2009. Observations are from Bikina et al. (2020). Model estimates of Test 0, Test 1, Test 2, and Test 3 were calculated along the cruise tracks using the IMPACT model. The Taylor diagram summarizes the statistics for the comparison between observations of aerosol Fe solubility and the different simulations (Test 0-3). The dashed curves in blue indicate the standard deviation values. The curves in red denote the root-mean-squared difference between the observational data and the model predictions (RMSE). The dashed lines in black represent the correlation coefficients.



85

Figure S4: Fe dissolution kinetics of Libyan dust end member in H₂SO₄ solutions at around pH 2 (open rectangles), with 1 M (NH₄)₂SO₄ (filled rectangles), with 0.01 M H₂C₂O₄ (open triangles), with 0.01 M H₂C₂O₄ and 1 M (NH₄)₂SO₄ (filled triangles). The molar concentrations of H₂SO₄, H₂C₂O₄ and (NH₄)₂SO₄ in the experiment solutions are shown. The final pH of the experiment solutions is also reported, which was calculated using the E-AIM model III for aqueous solution (Wexler and Clegg, 2002) accounting for the buffer capacity of the CFA samples (Experiments 1-4 in Table S1). The data uncertainty was estimated using the error propagation formula.

90

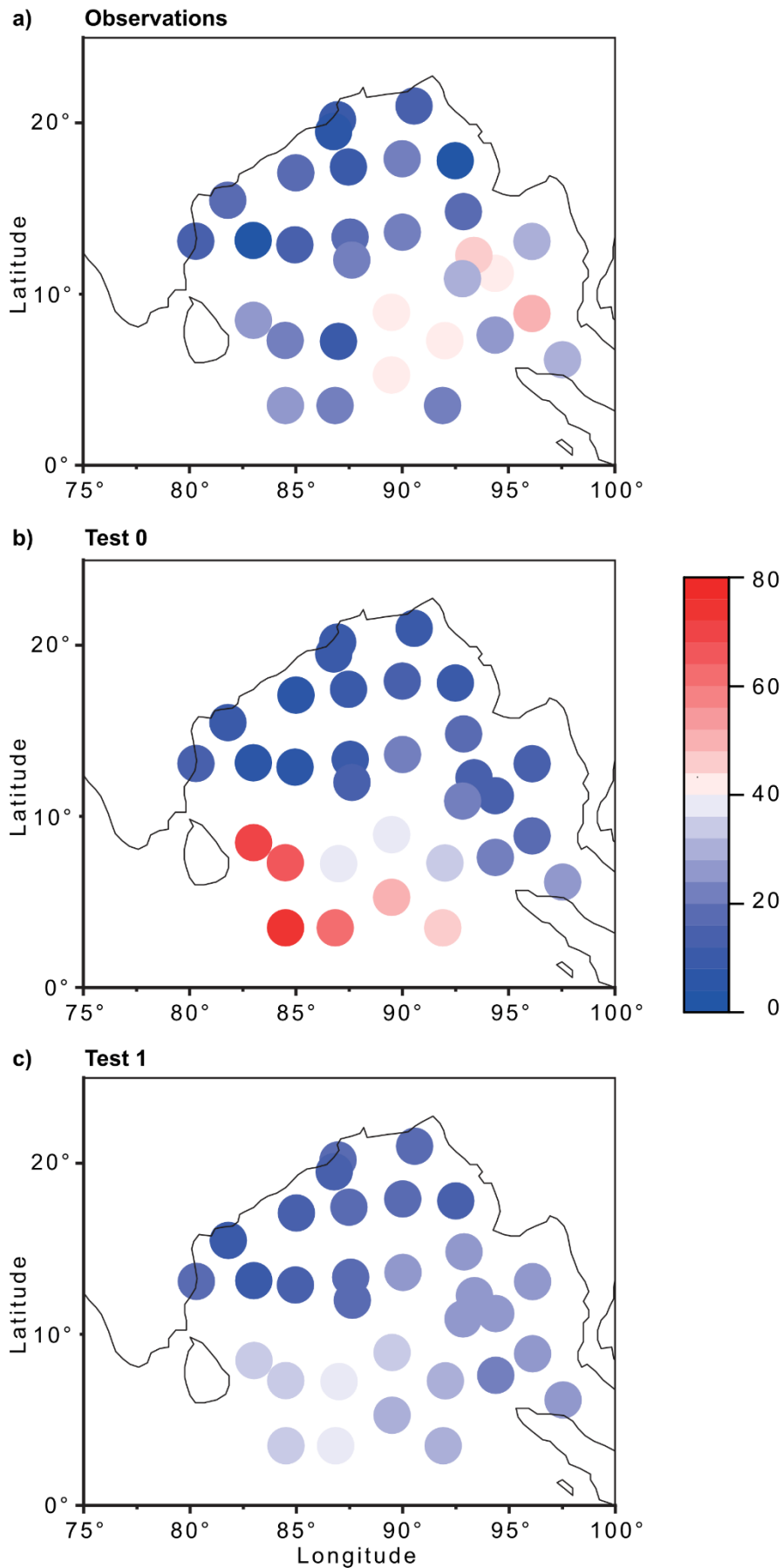


Figure S5: Fe solubility in PM_{2.5} aerosol particles over the Bay of Bengal from 27 December 2008 to 26 January 2009. a) Observations from Bikkina et al. (2020). b-c) Model estimates of Test 0 and Test 1 calculated along the cruise tracks using the IMPACT model. In Test 0, we ran the model without upgrades in the Fe dissolution scheme (Ito et al., 2021) and applying the proton-promoted, oxalate-promoted and photoinduced dissolution schemes for combustion aerosols in Table S6 (Ito, 2015). The proton + oxalate dissolution scheme (Table 1) was applied in Test 1 and we adopted the base mineralogy for anthropogenic Fe emissions (Rathod et al., 2020).

95

References

- 100 Bikkina, S., Kawamura, K., Sarin, M., and Tachibana, E.: ^{13}C Probing of Ambient Photo-Fenton Reactions Involving Iron and Oxalic Acid: Implications for Oceanic Biogeochemistry, *ACS Earth Space Chem.*, 4, 964-976, doi: 10.1021/acsearthspacechem.0c00063, 2020.
- Ito, A.: Atmospheric Processing of Combustion Aerosols as a Source of Bioavailable Iron, *Environ. Sci. Technol. Lett.*, 2, 70-75, doi: 10.1021/acs.estlett.5b00007, 2015.
- 105 Ito, A., Lin, G. X., and Penner, J. E.: Radiative forcing by light-absorbing aerosols of pyrogenetic iron oxides, *Sci. Rep.*, 8, 7347, doi: 10.1038/s41598-018-25756-3, 2018.
- Ito, A., Adebisi, A. A., Huang, Y., and Kok, J. F.: Less atmospheric radiative heating by dust due to the synergy of coarser size and aspherical shape, *Atmos. Chem. Phys.*, 21, 16869–16891, doi: 10.5194/acp-21-16869-2021, 2021.
- Rathod, S. D., Hamilton, D. S., Mahowald, N. M., Klimont, Z., Corbett, J. J., and Bond, T. C.: A Mineralogy-Based Anthropogenic Combustion-Iron Emission Inventory, *J. Geophys. Res.-Atmos.*, 125, e2019JD032114, doi: 10.1029/2019jd032114, 2020.
- 110 Wexler, A. S., and Clegg, S. L.: Atmospheric aerosol models for systems including the ions H^+ , NH_4^+ , Na^+ , SO_4^{2-} , NO_3^- , Cl^- , Br^- , and H_2O , *J. Geophys. Res.-Atmos.*, 107, 4207, doi: 10.1029/2001JD000451, 2002.